Heterodyne interferometer for detection of conditional single-photon phase shifts

Anna Karoline Speier

Bachelorarbeit in Physik
angefertigt im Institut für Angewandte Physik

vorgelegt der
Mathematisch-Naturwissenschaftlichen Fakultät
der
Rheinischen Friedrich-Wilhelms-Universität
Bonn

Feb 2023

Ich versichere, dass ich diese Arbeit selbstständig verfasst und keine anderen als die angegebenen Quellen und Hilfsmittel benutzt sowie die Zitate kenntlich gemacht habe.

Bonn, 16.2.23 .....A. Spier.....

Datum Unterschrift

1. Gutachter: Prof. Dr. Sebastian Hofferberth
2. Gutachter: Prof. Dr. Simon Stellmer

Contents

CHAPTER 1

Introduction

The interaction of light with matter forms our visual perception of the world and is therefore fundamental to the understanding of our surroundings. The properties of light are changed when it travels through a medium, depending on the material characteristics. The important property for describing light propagation is the refractive index of a medium, which describes the severity of the influence the material has on the light beam [1].

This refractive index depends not only on the properties of the propagated medium but also on the frequency of the light itself [2]. This relationship becomes critical for quantized-level systems for instance around atomic transitions. Especially in the case where multiple electromagnetic fields are applied like in electromagnetically induced transparency. Here the transmission of a weak input field is modified upon the presence of a second stronger light field. In such a three-level system the interference between two excitation pathways can lead to the controlled transmission of light [3].

The response of a medium can be, but is not necessarily, linear in relation to the light intensity. This is for instance the case for saturatable systems, such as systems of Rydberg atoms where even a single photon can varry the medium for the next photon [4]. The resulting modification of the refractive index, which is in correlation to the susceptibility, can be used to realize light-based operations down to single photon level such as switches and phase gates [5–8].

In comparison to absorption, which is easily measured, determination of the phase shift introduced by a medium can not be achieved by measuring the light directly since optical frequencies of hundreds of THz cannot be detected by modern electronics and instead requires e.g. interferometry. There are two different phase shifts that can be measured: the unconditional phase shift which is the single photon phase, and the conditional phase which is the non-linear phase [9, 10]. Up until now in our research group, there were only interferometer setups that can detect the unconditional phase [11, 12].

The topic of this thesis is to build and characterize an interferometer, which in the end is designed to measure the conditional phase. To reach this goal, the setup discussed in the master thesis of Tomer Zohar was used as a guideline [13]. Their interferometer was recently used to show strong photon-photon interaction in a quantum nonlinear optical medium by measuring phase accumulation for co-propagating [14].

The focus of my thesis is the characterization of the setup stability and benchmarking the system by measuring linear phase shifts. The thesis is structured as follows: Chapter 2 discusses the interferometer setup and the theory behind interferometry. Chapter 3 describes the characterization of different aspects of the setup, including the stability on experimentally relevant timescales (hundreds of ms) and beyond (up to 120 s). Finally, Chapter 4 discusses the results and gives an outlook on possible improvements and implementation of the interferometer setup.

CHAPTER 2

Setup and theory

This section describes the built setup and its components while explaining interferometry in a classical picture starting with the Maxwell equations and the theory behind beat notes. The general design of the interferometer follows the thesis of Tomer Zohar [13] with adjustments to our components and circumstances. Finally, the concept of testing the interferometer and a possible reference beam will be discussed.

2.1 Basic interferometer

An interferometer is a setup that uses interference between two waves for measuring quantities of a signal. Figures 2.1 and 2.2 show examples of different types of interferometers. This will later be discussed in more detail.

In interferometry, there are different types of measurement depending on what signal interfere. Normally one distinguishes between homodyne and heterodyne detection. The names refer to whether two identical signals or two different signals are compared. Even though in our setup both beams have

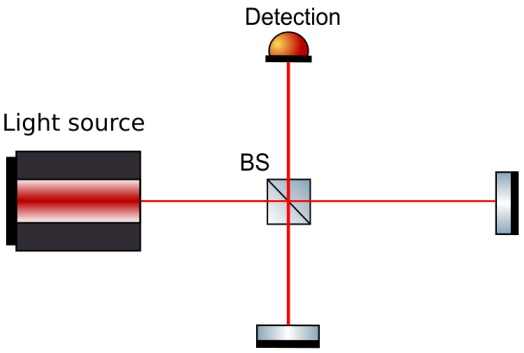

Figure 2.1: Basic setup of one type of interferometer (Michelson interferometer).

the same initial origin and result from splitting a single beam, our interferometry can be considered heterodyne. This is achieved as both arms are modified, which transforms the reference arm to be significantly different enough from the signal arm to call it a local oscillator (LO).

In the following sections, classical interference of light is introduced starting with the Maxwell equations.

2.1.1 Classical interference

This section is based on the explanation from the book 'Quantum Optics: an introduction' by Fox [15]. The Maxwell equations of electromagnetic waves are the basis to describe light fields, the relation between electric and magnetic field and their interaction with matter. $\mathcal{E}$ is the electric field and D is the electric displacement. H is the magnetic flux strength, while B describes the magnetic field.

$$\nabla \cdot D = \rho \tag{2.1}$$
$$\nabla \cdot B = 0 \tag{2.2}$$
$$\nabla \times \mathcal{E} = -\frac{\partial B}{\partial t} \tag{2.3}$$
$$\nabla \times H = j + \frac{\partial D}{\partial t} \tag{2.4}$$

The solution to this set of equations can be a transverse wave. When the electric field is along the x-axis, the solution is as follows:

$$\mathcal{E}_x(z,t) = \mathcal{E}_{x0}\cos(kz - \omega t + \phi) \tag{2.5}$$
$$B_y(z,t) = B_{y0}\cos(kz - \omega t + \phi). \tag{2.6}$$

ϕ is here the optical phase and k is the wave vector, which can be calculated by the wavelength of light in the medium λ_m:

$$k = \frac{2\pi}{\lambda_m}. \tag{2.7}$$

In terms of light waves one important quantity is the intensity of the wave, which is proportional to $\langle \mathcal{E}(t)^2 \rangle$. This is the signal, which will later be detected.

For mathematical discussion, we take a look at a simple form of an interferometer, which is a Michelson interferometer shown in figure 2.1. Here a beam splitter (BS) combines two lights that travel different arm lengths L after being split up. The two light waves would result in the following outcoming light wave, assuming a linear polarized monochromatic wave:

$$\mathcal{E}_{out} = \mathcal{E}_1 + \mathcal{E}_2 = \frac{1}{2}\mathcal{E}_0 e^{i2kL_1} + \frac{1}{2}\mathcal{E}_0 e^{i2kL_2} e^{i\Delta\phi} = \tag{2.8}$$
$$\frac{1}{2}\mathcal{E}_0 e^{i2kL_1}(1 + e^{i2k\Delta L} e^{i\Delta\phi}) \tag{2.9}$$

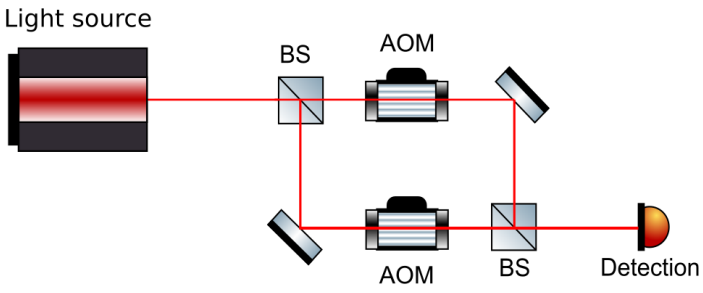

Figure 2.2: Sketch of the basic setup of the interferometer used in this experiment.

Here ΔL is the length difference between both arms and $\Delta\phi$ a possible phase change that can occur even when both arms have the same length. The field maxima and minima are then localizable via the following formula:

$$\text{Maxima: } \frac{4\pi}{\lambda}\Delta L + \Delta\phi = 2m\pi \tag{2.10}$$

$$\text{Minima: } \frac{4\pi}{\lambda}\Delta L + \Delta\phi = (2m+1)\pi. \tag{2.11}$$

With this exact mathematical calculation, one can determine the path lengths of the arms precisely by a measurement of the maxima and minima, which is one possible use of such an interferometer.

The interference described above holds for two general electromagnetic waves. For such interference to occur the light has to be coherent. Coherence describes the similarity and comparability of two light beams. The time during which the light beams are split has to be short enough. Else the quantities of the photons change too much and they do not interfere with each other anymore when the light beams are recombined. In an interferometer, this means that the paths have to be short enough. [1]

2.1.2 Interferometer setup

Figure 2.2 shows a simple sketch of the setup built for this thesis. The basic layout of the interferometer is called a Mach-Zehnder-Interferometer. In the built interferometer, the detected interference is created with two beams of different frequencies. In that case, the interference signal will carry a beat note. The following explanation about this comes from the book "Optics" by Hecht [1]. A beat note is the interference of a number of waves with different frequencies. As an example, there are two waves $\mathcal{E}_1$ and $\mathcal{E}_2$ with different angular frequencies $\omega_1 > \omega_2$ and resulting dissimilar propagation numbers $k_1 > k_2$ but the same amplitude $\mathcal{E}_{01}$. The resulting wave is then:

$$\mathcal{E} = \mathcal{E}_{01}(\cos(k_1 x - \omega_1 t) + \cos(k_2 x - \omega_2 t)) \tag{2.12}$$

$$\Rightarrow \mathcal{E} = 2\mathcal{E}_{01}(\cos(\frac{1}{2}[(k_1+k_2)x - (\omega_1+\omega_2)t]) \times \cos(\frac{1}{2}[(k_1-k_2)x - (\omega_1-\omega_2)t])). \tag{2.13}$$

This can be rewritten with an average angular frequency $\overline{\omega}$ and a modulation frequency ω_m:

$$\overline{\omega} \equiv \frac{1}{2}(\omega_1 + \omega_2), \qquad \overline{k} \equiv \frac{1}{2}(k_1 + k_2), \tag{2.14}$$

$$\omega_m \equiv \frac{1}{2}(\omega_1 - \omega_2) \text{ and } \qquad k_m \equiv \frac{1}{2}(k_1 - k_2) \tag{2.15}$$

$$\Rightarrow E = 2\mathcal{E}_{01}\cos(k_m x - \omega_m t)\cos(\overline{k}x - \overline{\omega}t). \tag{2.16}$$

This wave function can be described as one traveling wave with the angular frequency $\overline{\omega}$ whose amplitude is a modulated wave with the angular frequency of ω_m:

$$\mathcal{E}(x,t) = \mathcal{E}_0(x,t)\cos(\overline{k}x - \overline{\omega}t) \text{ with: } \mathcal{E}_0(x,t) = 2\mathcal{E}_{01}\cos(k_m x - \omega_m t). \tag{2.17}$$

In the relevant case of optical frequencies both ω_1 and ω_2 are large but close to each other, so that $\overline{\omega} \gg \omega_m$. The traveling wave is then a fast signal and the amplitude modulation is slow in comparison. $\mathcal{E}_0^2(x,t)$ oscillates with the beat frequency, which is

$$2\omega_m = (\omega_1 - \omega_2). \tag{2.18}$$

Up to now only the case of the waves with the same amplitude was described. When this is not the case the interference would still result in a beat but there would not be a complete extinction at the lowest points, and with that less contrast.

For the experimental setup the two beams were split from the same laser source, an extended cavity diode laser with a wavelength of 780 nm, which is the same wavelength as will be used later in the experiment. Generating the signals from the same laser has the advantage of having automatically two coherent signals. The different frequencies of the two beams, which are needed for the beat note, are created by passing each beam through an acusto-optical modulator (AOM) [16]. After this modulation, the beams are overlapped on a beamsplitter and the resulting beat note is detected.

2.1.3 Setup implementation of beat note

As previously described, the AOMs are needed to modulate the frequency of the passing light to create a beat note. As a driver of the AOMs a direct digital synthesizer (DDS) board is used. One AOM modulates to a frequency of 80 MHz and the other one modulates to 82 MHz so that a beat frequency of 2 MHz is created when using the same diffraction order from both AOMs. Because of the resolution of the DDS frequency, these frequencies slightly differed from the entered numbers and are only accurate up to the eighth decimal place.

Initially, the signal was detected on a photodiode and recorded on an oscilloscope.

2.1.4 Classical beat note

The used photodiodes were amplified SI free-space photodetectors [1]. The output signal from the photodiode is a voltage proportional to the incoming light intensity. This is then connected with an

[1] Thorlabs PDA10A2

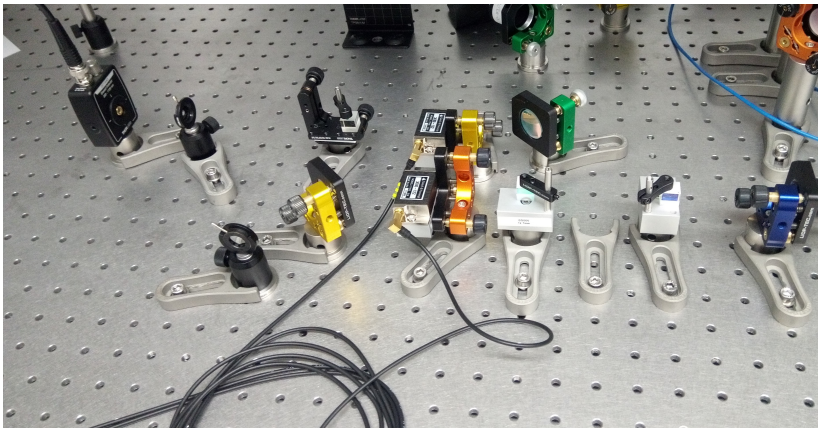

Figure 2.3: Picture of the setup of a simple form of the interferometer.

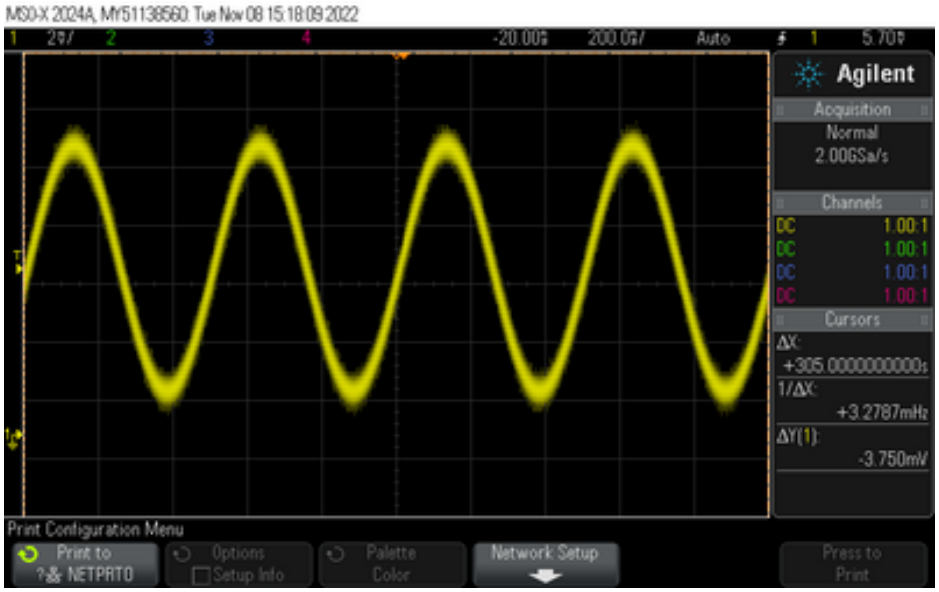

Figure 2.4: Beat signal on classical level detected by a photodiode.

oscilloscope. For the first iterations an Agilent MSO-X 2024 A was used. Here photos were captured from the display and the data were acquired mostly via the ethernet connection. At later stages a LeCroy Wavepro 7 was used in order to record over longer times at high resolution. Here the data could be directly saved on the device and later transferred for advanced data processing. In figure 2.4 a picture of the beat signal at this stage can be seen. These first measurements gave an idea of the beat note on a classical level of light intensities.

The interference pattern in figure 2.4 showed the functionality of the interferometer. The next steps in the progress focused on a more advanced and improved setup.

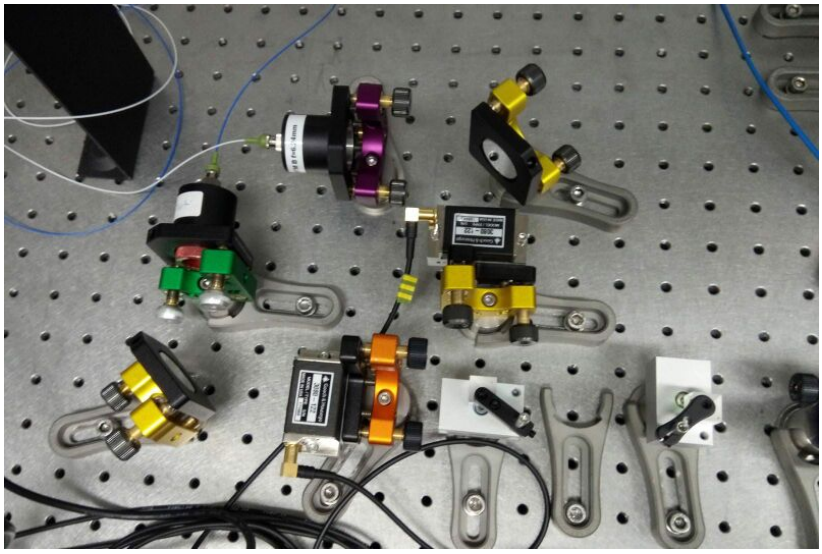

Figure 2.5: Picture of the setup of the interferometer with the fiber-beam splitter.

2.2 Advanced setup with focus on the stability

The beat note shown before illustrates that interference is observable with the setup. However, only a short timescale is depicted here. In reality, interferometers are sensitive to many perturbations, which will occur at some point when looking at longer timescales than just a few periods. For instance, a change in path length in one interferometer arm translates into a phase change at the detector. Therefore an unstable path length leads to instability as the contrast of the interference signal washes out over time. This is especially critical when long-time measurements are needed, which is the case for the measurement on a single photon level.

Efforts to minimize these effects were, in the first step, to reduce the size of the setup and, in the following step, to improve isolation from the surroundings. For these implementations, a few changes had to be made, which made the setup more complicated. This includes additional optical fibers and special components like an outer box for the reduction of outer influence primarily airflow. Additionally, the free space beam splitter that mixes the signal which has passed through the phase-modifying medium and the local oscillator signal was exchanged by a fiber beam splitter [2]. This implementation stage can be seen in figure 2.6.

By using a fiber-beam splitter the optical path in free space is reduced and the overlap between both beams can be maximized. To avoid loss of the signal light a fiber with a 99:1 mixture was chosen. The amplitude of the local oscillator was modified accordingly. To ensure overlap a polarization-maintaining beam splitter is used.

[2] Thorlabs PN780R1A2

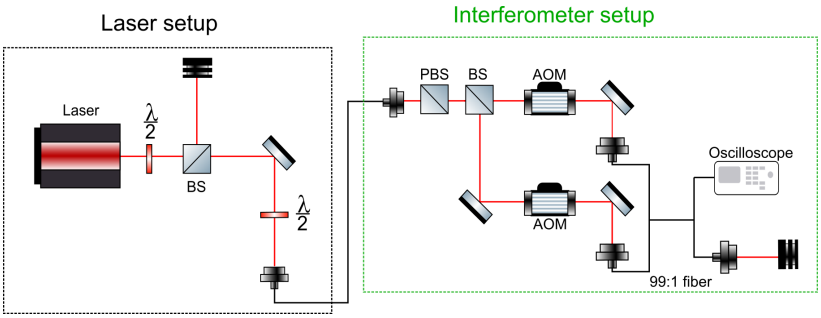

Figure 2.6: Sketch of the setup of the advanced interferometer.

2.3 Single photon measurement

After observing the classical interference signal and optimizing the stability of the setup, the detection method was switched from the classical light level measurement to a single photon level. For this, the photodiode was replaced by a single photon counting module (SPCM) to detect the beat signal.

2.3.1 Detection and logging on a single photon level

To switch to single photon detection, the light is drastically reduced via filters on both arms before going into the connected SPCM [3]. The SPCM creates a voltage spike when an incoming photon is detected. This can be connected to a Time Tagger [4], which registers the times of the incoming signal. The Time Tagger offers multiple different ways of saving the time stamps, including through a browser GUI [17]. The first technique to save the data was to have evenly spaced bins, which gets filled when a pulse arrives. As later there was a need for longer measurements and this method uses a lot of memory storage, a more efficient saving method was implemented. Here only the timestamps of arriving pulses are registered and saved. With this longer measurements of around 2 minutes were possible. For the device rms jitter is 34 ps according to the specifications [18].

2.4 Imitation of phase detection in an atomic sample

As a last modification of the setup an electro-optical modulator (EOM) was introduced to simulate an atomic medium where a phase shift is applied. The EOM modifies the phase and thereby allows testing if the interferometer is capable to measure a phase change. Therefore it was inserted into the probe arm. The full layout can be seen as a sketch in figure 2.7 and with a picture of the real setup in figure 2.8. In the photo an additional reference beam can be seen, which is split after each AOM and overlapped by a beam splitter. This way an optional reference signal can be obtained, but it will not be discussed further and is only an optional possibility to explore in a later upgraded version.

The EOM changes the phase of light passing through the EOM crystal [16]. Hereby the phase shift depends on the applied electric field. Therefore we apply a high-voltage signal, which switches between low and high voltage. The high voltage was supplied by a high-voltage power supply. There

[3] Laser Components Count-250C-FC
[4] Swabian Instruments Time Tagger 2.0

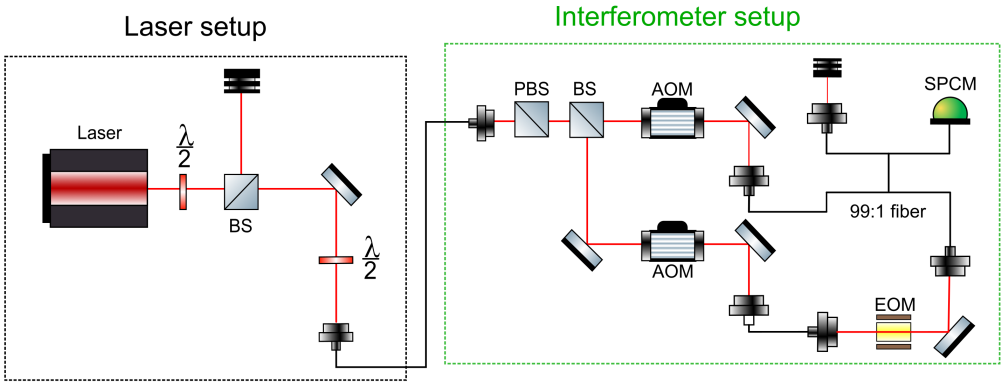

Figure 2.7: Sketch of the full setup.

is an additional function generator that is generating a square signal with a certain voltage and a specific period which is sent as a trigger signal to the switch to control it. When the voltage is raised, the switch is turned on and a phase change is applied to the light via the EOM. If the signal is off, the light continues through the EOM with no modification. The EOM repeatedly switches between On and Off with a rate determined by the frequency of the square signal on the function generator.

A phase shift is a relative quantity. In order to measure the shift caused by the EOM, the EOM is used in a pulse mode. The phase of the interference signal before and after applying the electric field is compared to get a reference, but this pulse can not be utilized as a trigger and is therefore not a reference signal.

A reference signal is in general useful for determining both drifts of the interferometer and atom-induced phase shift. One approach to achieve this is described in the following section.

2.5 Reference signal

An obvious candidate for a reference can be generated by using the direct interference signal between the DDS board's RF output signals. For that, we use the two remaining outputs of the DDS board and mix these electronic signals together, to create the same frequency as the interference of the two other

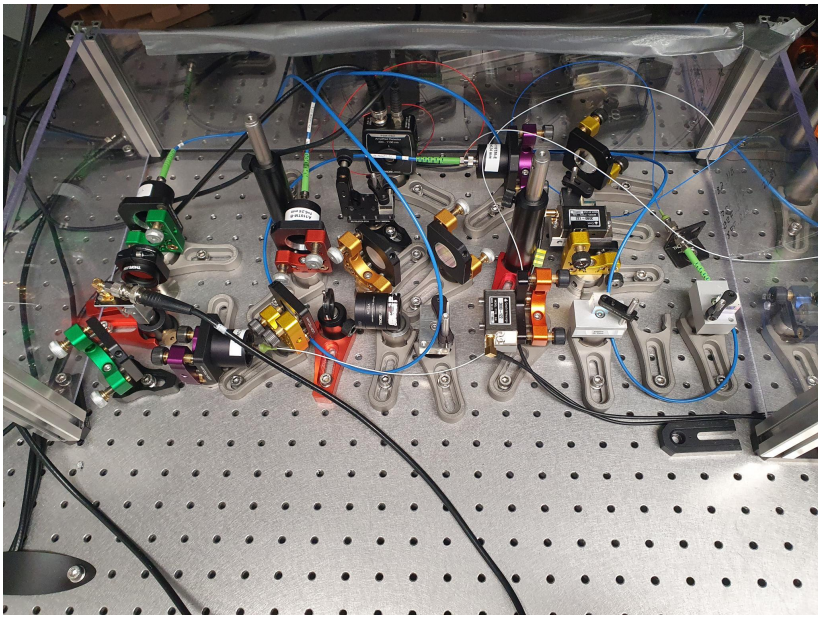

Figure 2.8: Picture of the full setup.

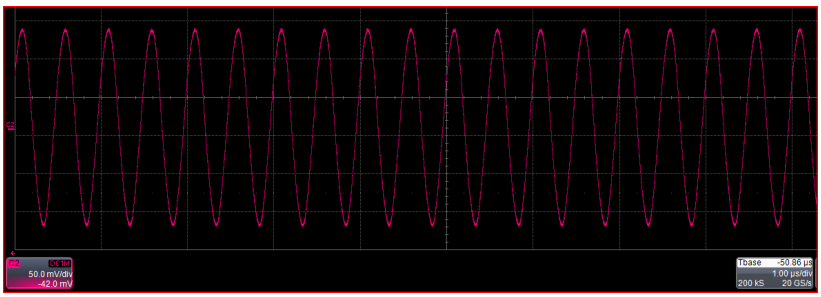

Figure 2.9: Reference RF signal on the oscilloscope after the mixer.

channels. A multiplying mixer connects the two outputs, which are set to the same frequencies as the first two channels used by the experiment namely 80 and 82 MHz. The output of the mixer is a signal which contains the sum and the difference between the input frequencies. A low-pass filter is used downstream to remove the high 162 MHz frequency and only pass the low frequency of 2 MHz. The resulting signal was a deformed sinusoidal. The intensity of this signal and to some degree the deformation can be controlled by changing the relative intensity of the two RF signals, with the result in figure 2.9. When the method of measurement was in the later stages of the project changed to the Time Tagger, it was necessary to introduce an extra modification on the signal as for the Time Tagger the incoming signal should only have positive values. This was fulfilled by the use of a bias tee, which connected with an additional constant voltage by a function generator, raises the offset of the signal above 0 V. Additionally the signal needed to be modified closer to a square signal than a sinus curve since it is used as a trigger signal and the Time Tagger has problems with continuous signals. Hence the signal is further passed through a comparator circuit which turns an analog sinusoidal signal into square TTLs. This device is discussed in the masterthesis of Mikkel Gaard Hansen [12]. With these

alterations, the signal can be measured with the Time Tagger and could possibly be used as a trigger if it is a suitable reference signal. The characteristics of this reference signal will be discussed further in the following chapter.

CHAPTER 3

Interferometer characterization

This chapter discusses the performance of the built interferometer described in chapter 2. For the characterization of the interferometer, the interference signal is measured and evaluated.

First, an explanation for the data processing method is given, before the beat note of the DDS RF signal is investigated by this method. Then the single photon interference signal is considered, in particular with focus on the stability over longer times. Finally, a phase-changing medium is simulated with the EOM and the result is presented.

3.1 Folding method

In the following section, the considered data consists of timesstamps of single photon events. The rate of photons arriving at the SPCM is low compared to the 2 MHz beat signal, with on average 1.47 photons per period. Therefore, in order to observe and measure the interference signal, it is necessary to post process the data. This is done by 'folding' the observed events in a specific time interval onto itself with a single period time. This procedure is sketched in figure 3.1 with example data that is not measured by our interferometer. The first graph 3.1(a) shows 5 periods of the oscillating signal which is illustrated by the sinusoidal envelope. During this time interval some individual events occur, which are selected with a certain probability from the sinus wave. The black vertical lines show the division into different periods.

These events are now taken modulo the period time to fold the signal of longer time spans onto itself in one wave period. The graph 3.1(b) shows the histogram over 5 periods. Here no clear distribution is visible. This changes with the graph in figure 3.1(c) where 500 periods are folded. The sinusoidal signal starts to get visible.

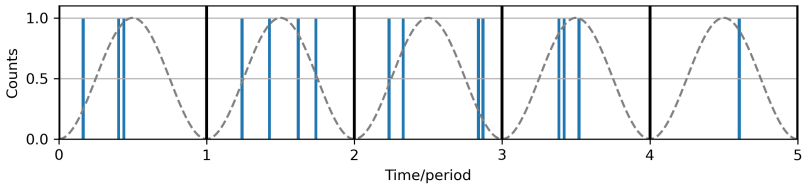

(a) Example data to illustrate the raw data of a single photon measurement with the dashed sinus curve the singular events are randomly selected from and the black lines to illustrate the periods.

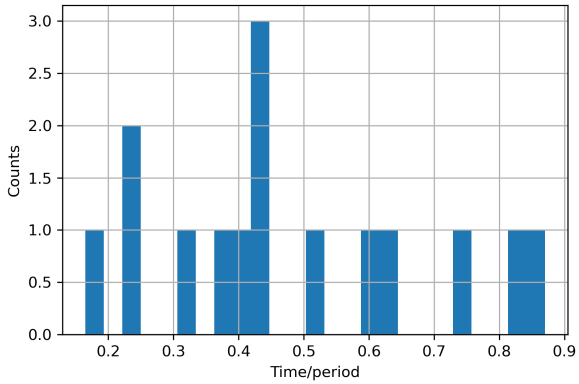

(b) Histogram of the example data folded onto itself over a time span of 5 periods.

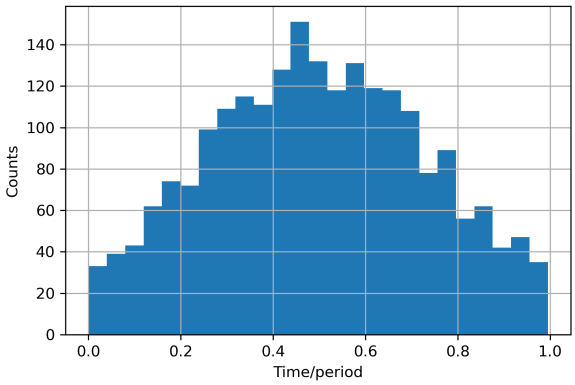

(c) Histogram of the example data folded onto itself over a time span of 500 periods.

Figure 3.1: Folded data of the reference signal.

This example shows how to get from a single photon measurement to a periodic signal by iterating it over longer measurement times and folding the data onto itself. In the following sections the method will be used with the real measured data.

3.2 Reference signal

As discussed in section 2.5 a beat note signal was created between two empty channels on the DDS board driving the two AOMs in the interferometer. This signal is tested as a candidate for a suitable reference signal.

A constant phase drift of the folded data made it clear that the exact period time was difficult to obtain as it slightly differed from the entered 2 MHz. To examine if the signal coming from the DDS board would be a suitable option as a reference signal it was measured with the Time Tagger. 5 μs of the raw data are shown in figure 3.2.

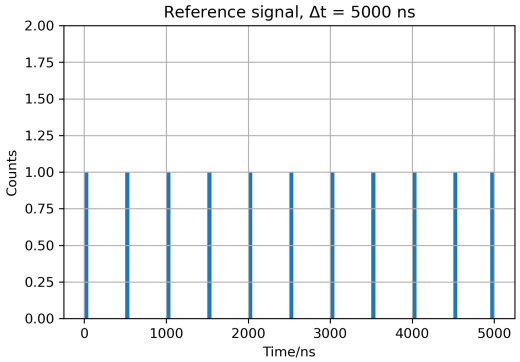

Figure 3.2: The data acquired by the Time Tagger for the reference signal over time.

Here the detector recorded a signal with an approximated frequency of 2 MHz, which is a period of $T = 500$ ns. With the data of the timestamps over 10 s, a mean value of the differences between the events was calculated as the period of the sinus function.

$$T = 500.101616 \text{ ns} \Rightarrow f = \frac{1}{T} = 1999593.61859 \text{ Hz} = 1.99959361859 \text{ MHz} \tag{3.1}$$

This calculation showed that the frequency is close to the expected 2 MHz and varies after the fifth decimal place.

With this period the data was then folded and plotted again in histograms for different lengths of time. The results are displayed in figures 3.3(a)-3.3(c).

For the foldings of 100 ms and 1 s all counts fell in a small time range of around 4 ns as can be seen in the figures 3.3(a) and 3.3(b). However, the shape is not as expected from folding a perfect periodical signal. A perfect periodical signal would create a single bin. If it jitters randomly with a uniform distribution, a Gaussian would be expected. This is more of a two-peaked distribution, which illustrates not perfectly random jitter. The data processing was not the cause of this form since the data presented by the Time Tagger GUI showed the same behaviour, shown in figure 3.4. The shape did not improve with other close numbers for the period, where the width of the shape only got wider. This observed two-peaked shape is caused by the comparator used to turn the sinusoidal into a square

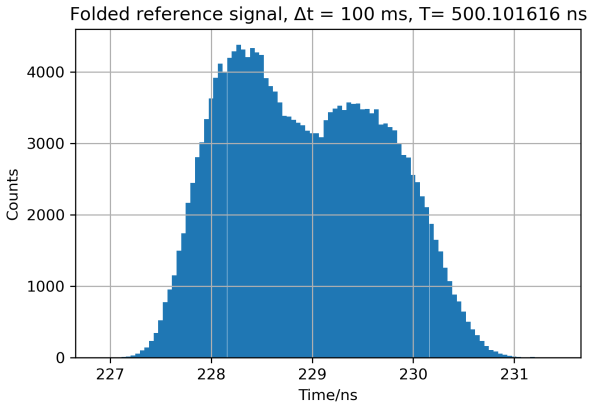

(a) Folded data of the reference signal for 100 ms with the calculated period.

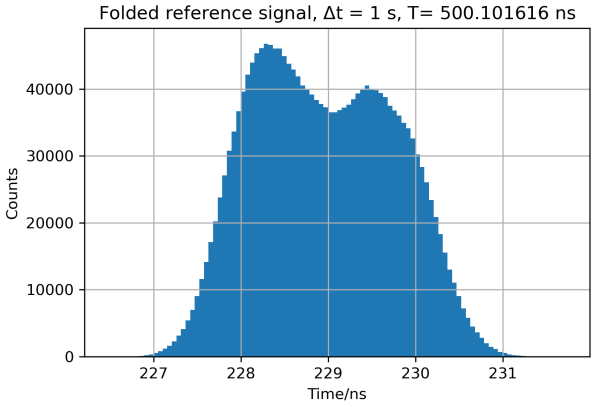

(b) Folded data of the reference signal for 1 s with the calculated period.

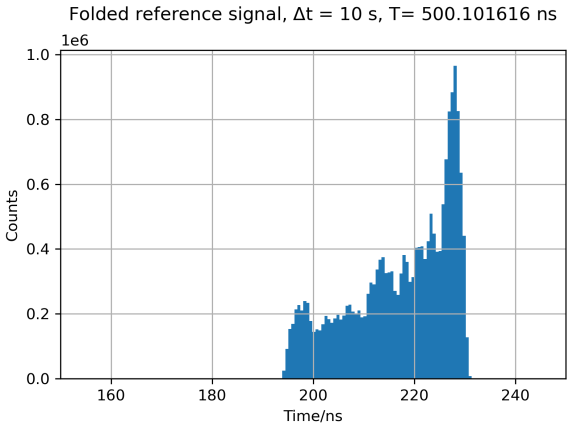

(c) Folded data of the reference signal for 10 s with the calculated period.

Figure 3.3: Folded data of the reference signal.

waveform. This is caused by the limitation of the slope straightening, as it still remains smooth to a degree. While the signal with the used device showed a better performance than just the signal, when considering this, the device still has a limited precision on smooth curves as we use one here.

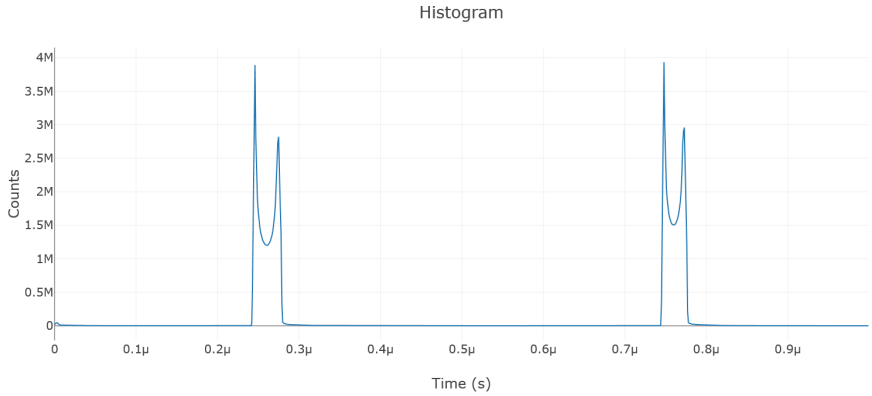

Figure 3.4: Reference signal viewed on the Time Tagger GUI as a histogram.

Now it can be considered whether the calculated period is a good estimation for the folding as the shape is a result of the data and the measurement method, then it seems to be a stable frequency over times of the order of one second. However, it is not stable over longer times as can be seen in the washed out figure 3.3(c) with a much wider distribution when measured for 10 s.

3.3 Interferometer data

Now we take a look into the data of the optical beat signal from the interferometer. As shown in section 2.1.3 an interference signal on a classical level was captured. This also appears in the data from the TimeTagger GUI when measured with the SPCM, as shown in figure 3.5. Here the figures shows the histogram of detection events compared to an initial detection event. One can see the dead time of the SPCM and oscillations on two different time scales.

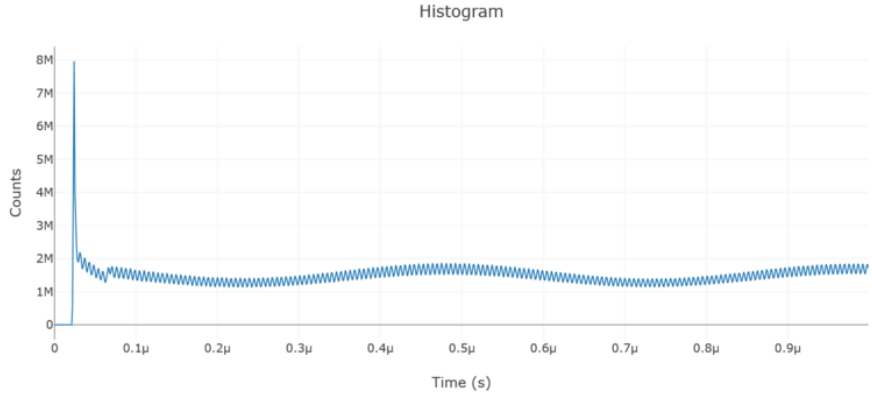

Figure 3.5: Beat signal on few photon level detected by a SPCM and represented in the Time Tagger GUI.

The fast oscillation is most likely caused by ringing in the SPCM signal and is only visible because of the representation of the data. The fast oscillation also appears in the dark count measurement.

With the visible periodic signal of around $f = 2$ MHz shown in figure 3.5, we would expect to find an oscillation of the single photon counts in a folded long trace measurement. To test this, the signal from the setup was folded by the same period that was calculated for the reference signal. The resulting detection-time histogram can be seen in the figures 3.6-3.9 for total measurement durations of 10 ms, 100 ms, 1 s and 10 s.

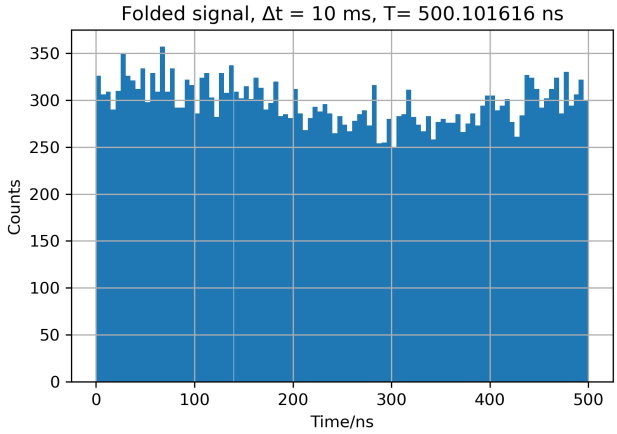

Figure 3.6: Folded single photon detection time data of the signal for 10 ms with the calculated period.

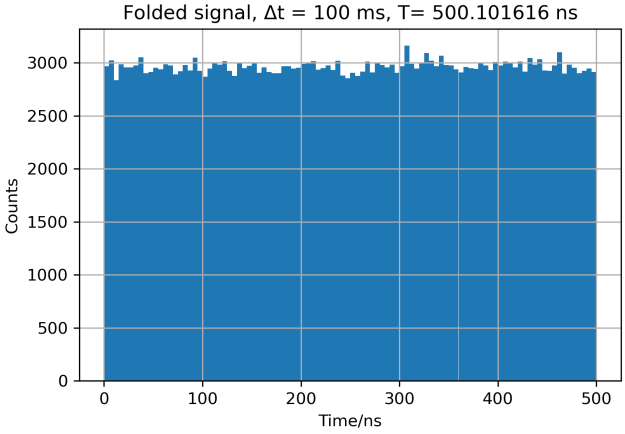

Figure 3.7: Folded single photon detection time data of the signal for 100 ms with the calculated period.

With this period time a low contrast modulation is visible when the first 10 ms of the data set are considered. For longer times no sinusoidal signal can be extracted. Therefore this period does not work for the signal from the setup and the 'reference' signal can not be used as such.

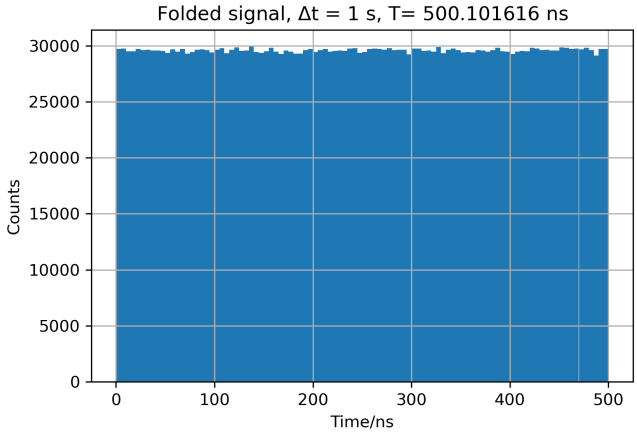

Figure 3.8: Folded single photon detection time data of the signal for 1 s with the calculated period.

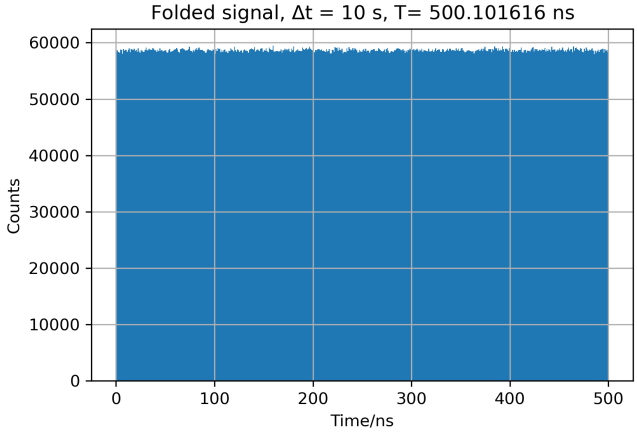

Figure 3.9: Folded single photon detection time data of the signal for 10 s with the calculated period.

Instead of using the reference period, an iterative method was applied, trying out different period times and evaluating their performance over increasingly longer measurements. This way the period time was optimized for our data. Through this, a period of T=500.0721 ns was found.

The periodic signal of the folded data can be seen in figure 3.10.

To see how the reference signal responds to the chosen period of the interference signal, the reference data was folded by that period. This created the figures 3.11-3.14.

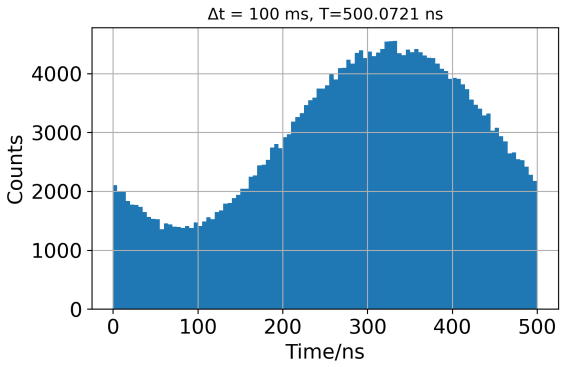

Figure 3.10: Folding of the interferometer signal by T=500.0721 ns.

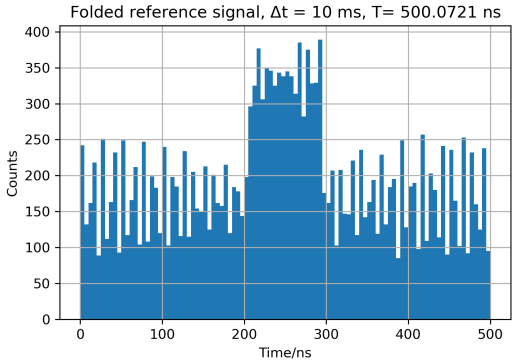

Figure 3.11: Folded data of the DDS reference signal for 10 ms with the calculated period of the setup signal.

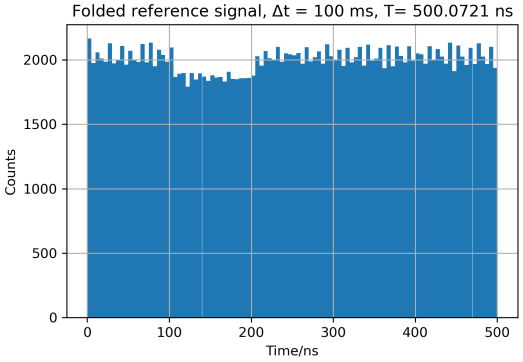

Figure 3.12: Folded data of the DDS reference signal for 100 ms with the calculated period of the setup signal.

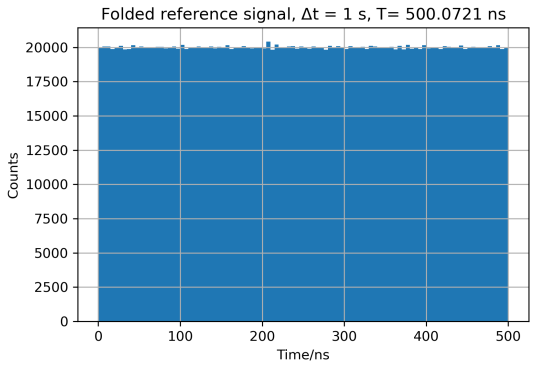

Figure 3.13: Folded data of the DDS reference signal for 1 s with the calculated period of the setup signal.

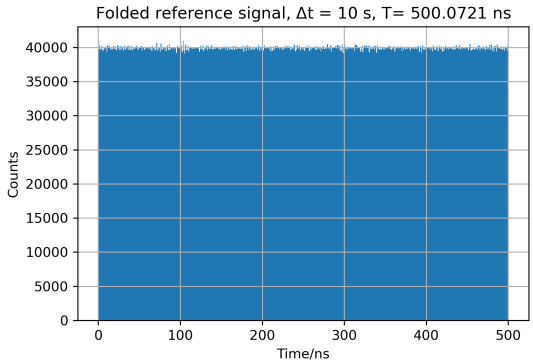

Figure 3.14: Folded data of the DDS reference signal for 10 s with the calculated period of the setup signal.

With the period extracted from the single photon data, the evenly spaced detection events shown in figure 3.2 run out of phase and the long time stability shown in figure 3.2 vanishes. Only at short timescales, it is visible that there is some data range, where the signal is not at the same level as the rest which has a distantly resemblance of a periodic signal. This washing out is similar to the one found when the interferometer signal is folded with the reference period. This shows that the exact period especially at a precision stage of a few decimal numbers, becomes important for longer times since a minimal longer or shorter period reinforces the effect of the small difference with every additional folding.

In figure 3.16 the Time Tagger data from the GUI can be seen, when the reference signal is used as the trigger of the histogram. Here no periodic signal is visible as the only noticeable pattern does also appear in the same measurement for the dark counts in figure 3.15.

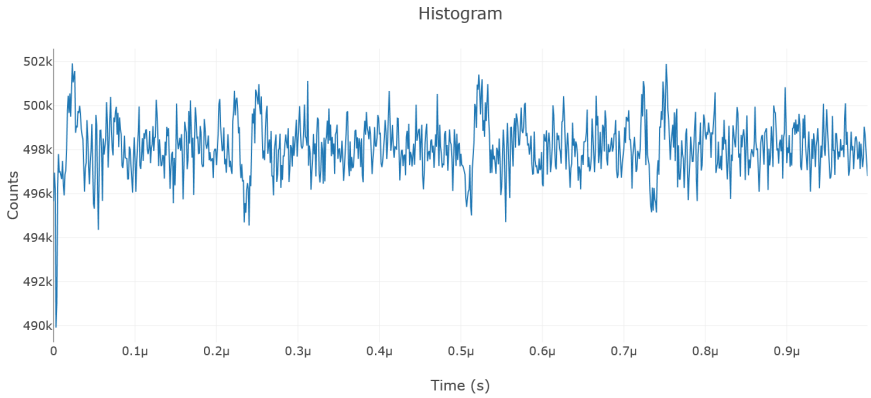

Figure 3.15: Dark count signal with the reference signal as a trigger.

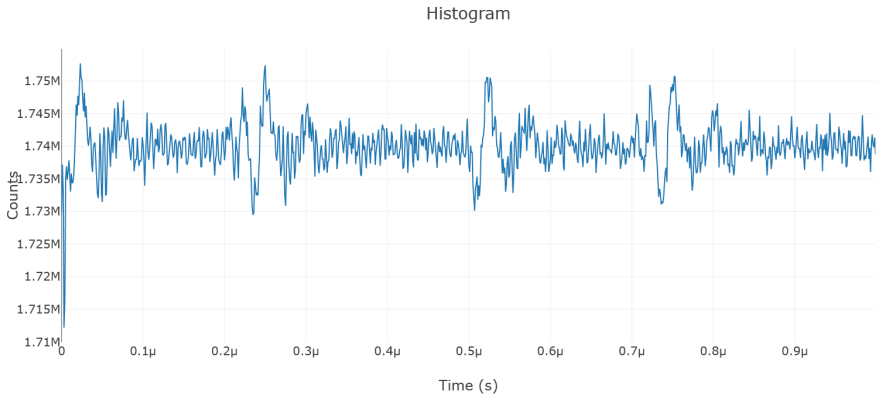

Figure 3.16: Interferometer signal with the reference signal as a trigger.

This cross-test showed here again that the periods for the electronic reference signal and the optical setup signal differ too much to be used as a reference.

3.4 Control signals

Figure 3.10 a good period time was found for the signal, producing a detectable oscillation of the single photon data over at least 100 ms. To check that the oscillation in the folded data is a result of the interference and does not come from other sources, different signals were measured. First dark count data without any laser light were taken and folded over 100 ms by T=500.0721 ns in figure 3.17.

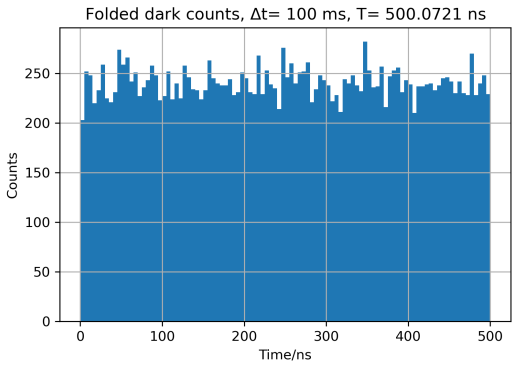

Figure 3.17: Darkcounts measurement without any laser light over 100 ms.

Here no oscillation was detected and therefore the periodic signal cannot stem from some dark-count effect or directly from the electronics. It was also checked whether some oscillatory signal is presented in the individual interferometer arms. For that, the signal of the arm where the probe will be located and of the LO arm were measured separately. If the oscillation comes from the interference one would not expect any periodic signal. The results in figures 3.18 and 3.19 show that the two arms measured separately the same constant distribution as the dark counts. The arms on their own are not the source of the oscillation which leads to the conclusion that the oscillating signal is the interferometer beat note signal.

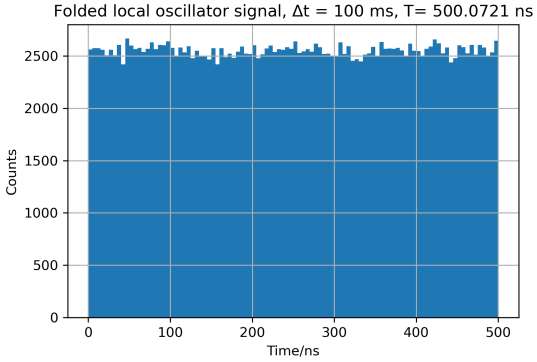

Figure 3.18: Local Oscillator arm measurement with a blocked probe arm over 100 ms.

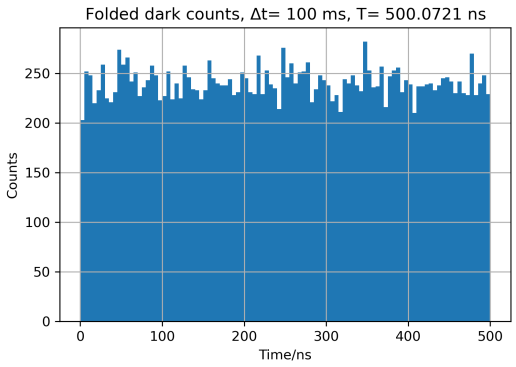

Figure 3.19: Darkcounts measurement without any laser light over 100 ms.

3.5 Beat signal characterization

Now that the oscillation is confirmed as the beat signal, this signal is characterized more carefully.

3.5.1 Fixed period

In figure 3.20 a snippet of the raw collected Time Tagger data can be seen. This shows that the photons are as expected not as evenly spaced in time as compared with the reference signal figure 3.2. Photons from a coherent light source follow a Poissonian time distribution [15]. This gives insight into the difficulties of calculating a possible phase shift as the distribution of the photon appearance seems random and only shows their periodic distribution over many iterations.

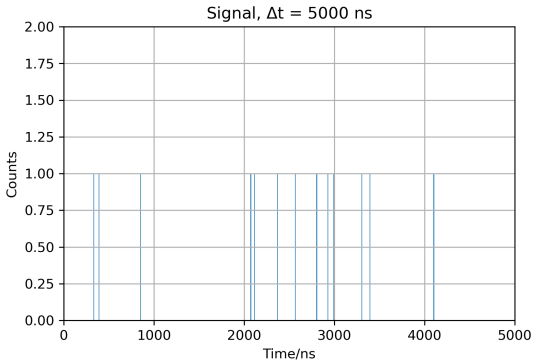

Figure 3.20: The data acquired by the Time Tagger for the signal over time.

To take a look into the stability of this chosen period the data was folded starting at three different times (around 0 s, 1 s, 9 s) for three different lengths (100 ms, 500 ms, 1s). The folding is depicted in figure 3.21. The period is a good fit for this timescale as the waveform does not wash out and instead has a similar depth at 0 seconds and at 9 seconds. It also is stable over 100 ms as well as 500 ms and even for 1 s.

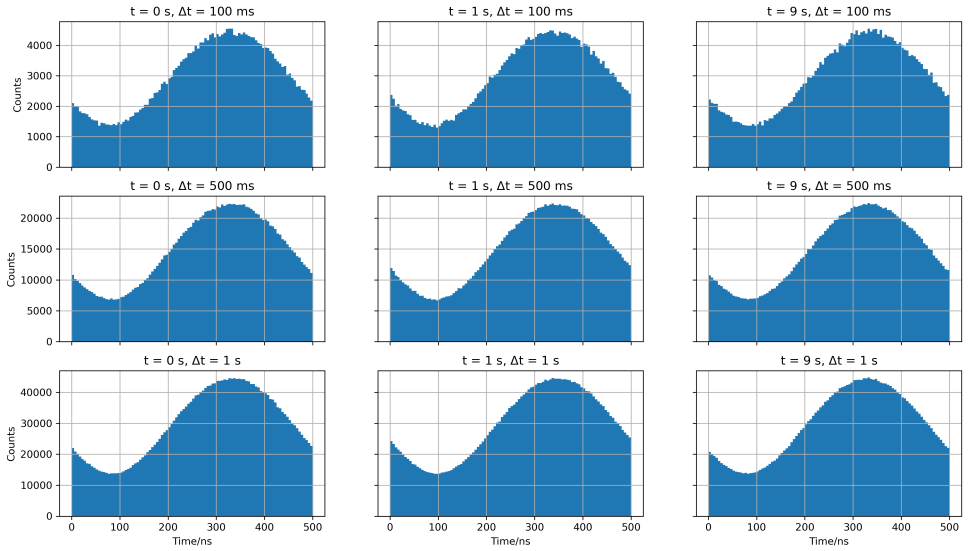

Figure 3.21: 3x3 grid with one length per row and at one time per column.

To have a better presentation of the evolution of the periodic signal over time, 1 second is split into 100 times 10 ms intervals in figure 3.22. These are folded and plotted as a heat map line in figure 3.22. The figure illustrates that the periodic signal of this measurement does not experience a phase shift over at least 1 s as no considerable drift of the amplitude becomes apparent.

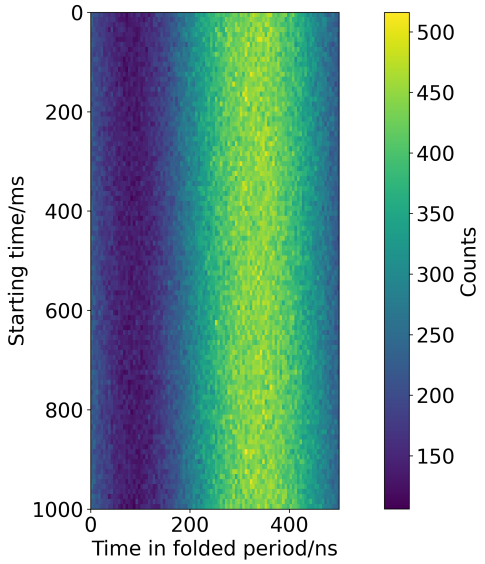

Figure 3.22: 100 times 10 ms snippets folded and plotted as a heat map.

3.5.2 Contrast

To quantify the stability, a sinus curve can be fitted to the histogram and then a contrast can be calculated from the parameters. The contrast C is defined by the proportion between the high points and low points, which are calculated by the offset O with added or subtracted amplitude A.

$$C = \frac{O + A}{O - A} \tag{3.2}$$

From this formula consequently, C=1 would be a bad contrast value, as there would be no oscillation visible. The higher the number, the better the contrast gets with this definition. The given errors are calculated from the covariance of the fit parameters.

This was again done for different time lengths of folded data between 0.1 ms and 10 s in figure 3.23.

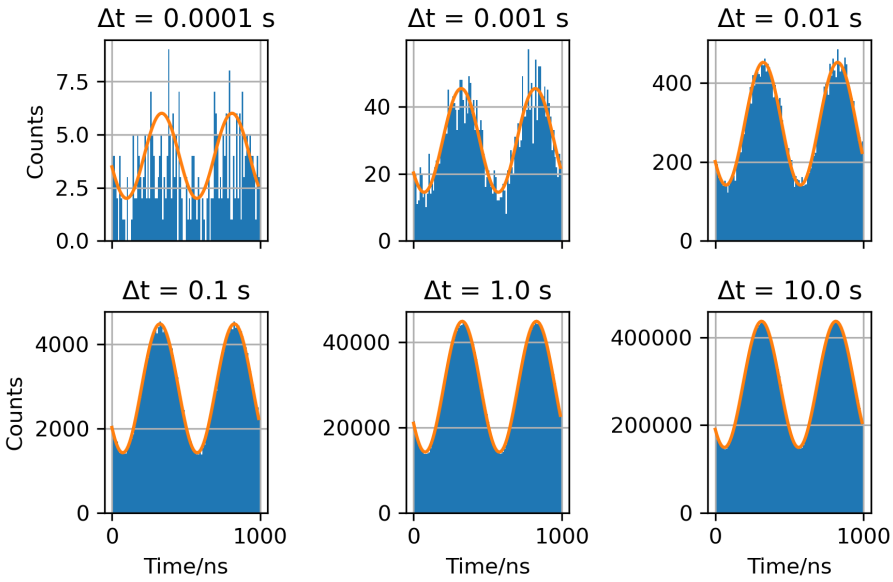

Figure 3.23: Folded data of different lengths with a fitted sinus function.

The calculated contrasts are plotted over a logarithmic timescale in figure 3.24. The differences of the contrast are in the range of 0.03, which is small compared to a real noisy system. Over every timescale tested here, the system seems to be rather stable. While having a lower contrast at the lowest and highest timescales, the highest contrast appears at 10 ms. 100 ms and 1 s are close by and show that the choice of period maintains the interference.

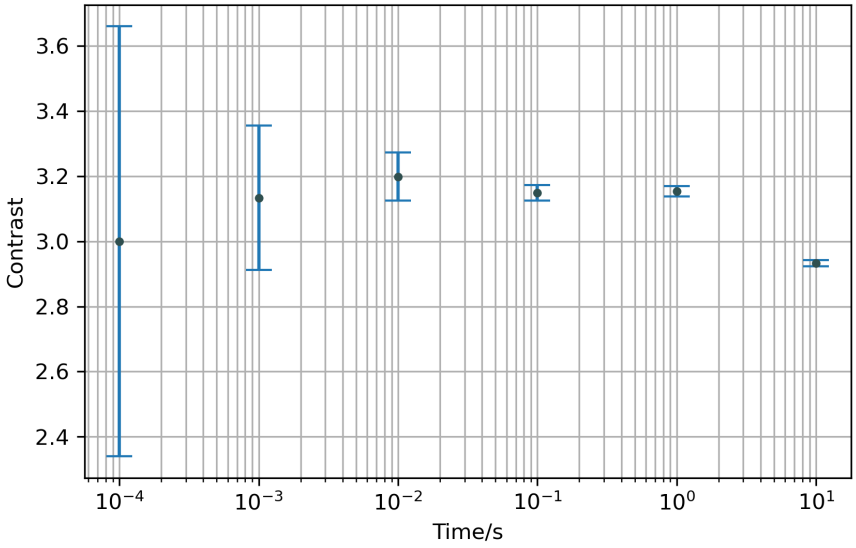

Figure 3.24: Plotted contrasts over different lengths of folding.

3.5.3 Stability of period

Contrast changing can also be an effect of a small mismatch between the folding period time and the actual interference period. Therefore we now consider the stability of the period and whether the choice of period changes over longer times. For this, a two-minute measurement was taken and the folding by the period to the first and the last second was applied. In figures 3.25 and 3.26 the folded data can be seen. For the first second the period used so far results in a high contrast histogram of the folded data, however, for the last second the contrast is lower and it seems that the period does not fit any more as properly. This can be caused by the period of the DDS board drifting or by instability of the timestamps.

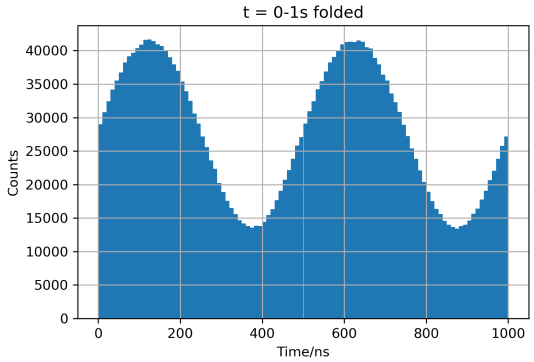

Figure 3.25: First second of the two minute measurement folded by chosen period time.

To take a closer look into finding a fitting period for this measurement, the first second was folded

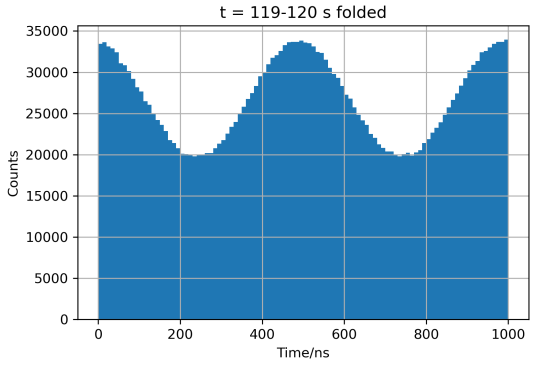

Figure 3.26: Last second of the two minute measurement folded by chosen period time.

over different periods. The histograms are shown in figure 3.27.

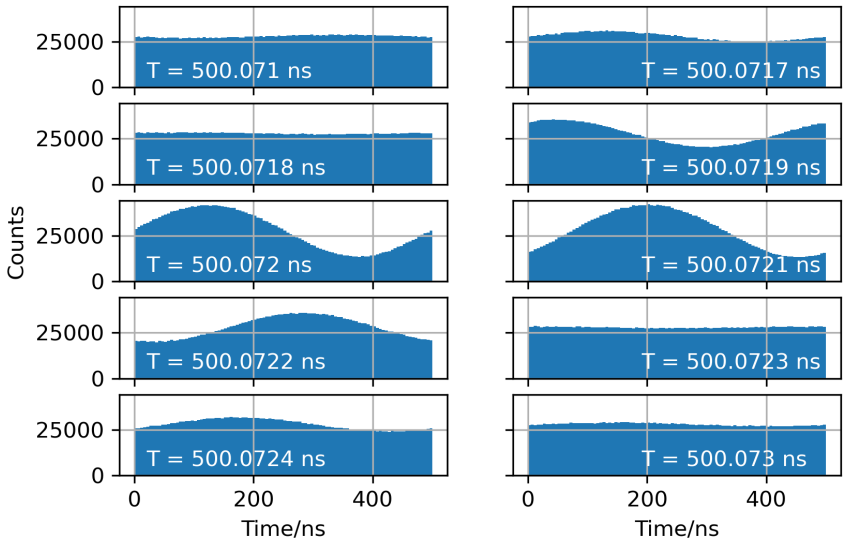

Figure 3.27: Analysis of the signal during the first second with respect to different periods.

The calculated contrast was the best for the T=500.0721 ns graph. It was slightly better than for the T=500.072 ns graph as can be seen in the below table 3.1 where all calculated contrast of these graphs are presented.

For the first second the T=500.072 ns period seems to be a good fit. Figure 3.28 shows how the contrast behaves over a timescale of up to 100 s, with the calculated contrasts plotted in figure 3.29. Here it gets better until 1 s, but halves from then to 10 s, with a peak developing. The contrast gets close to 1 for 100 s. The vast difference in this measurement compared to the contrast measurement in section 3.5.2 shows, that the change of the period has a huge influence on the washing-out effect. While having a similar good contrast at 1 s, the here observed low contrast at 10 s is probably a result

Table 3.1: Calculated contrast of different periods

T/ns	Contrast C
500,071	1.0614(17)
500,0717	1.2255(24)
500,0718	1.034(16)
500,0719	1.7238(30)
500,072	3.014(12)
500,0721	3.148(11)
500,0722	1.7812(33)
500,0723	1.0312(18)
500,0724	1.3139(21)
500,073	1.0731(18)

of a change in frequency and equivalently period.

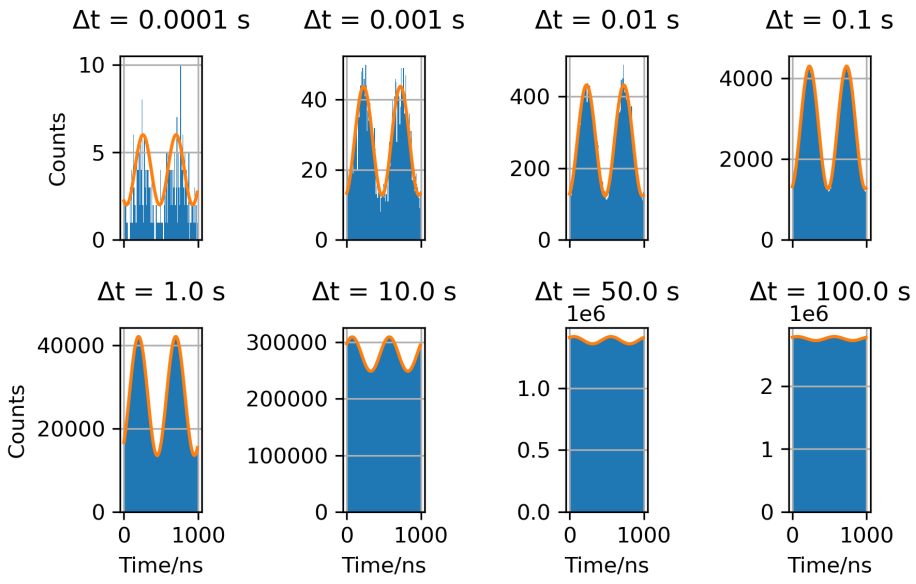

Figure 3.28: Folded data in different timescales up to 100 s.

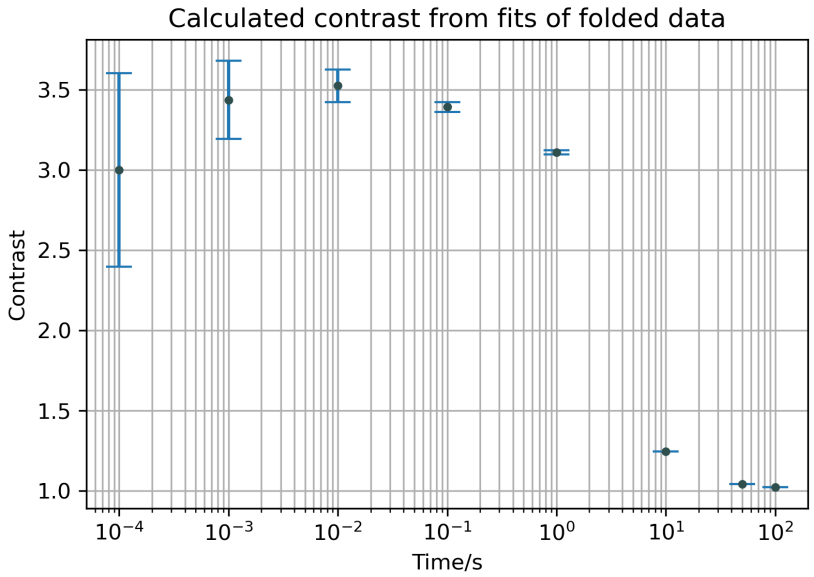

Figure 3.29: Contrast over different timescales for 120 ms measurement.

To now compare whether a change of frequency could be a reason for the washing out the first and last seconds are plotted in figure 3.30 with different folding times. Between the first and the last second are 119 seconds.

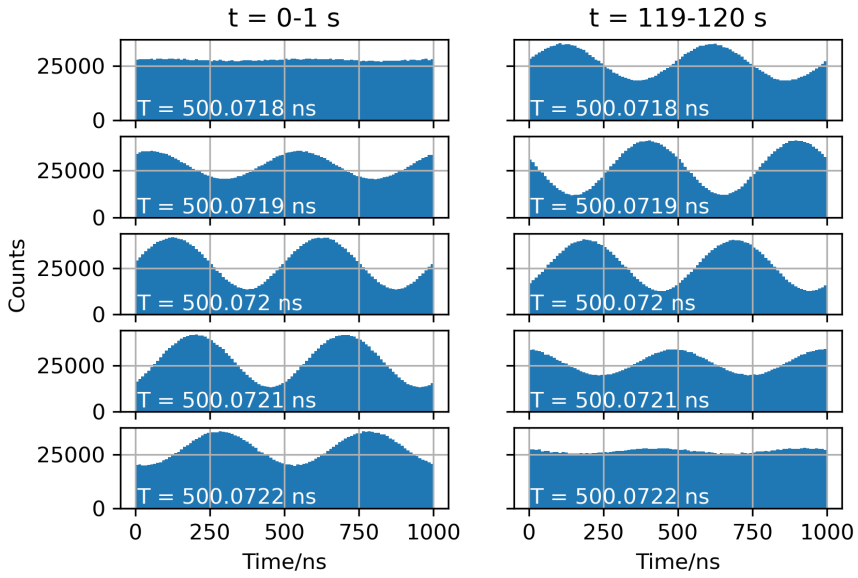

Figure 3.30: Both selected times folded by different period times. The period times were multiplied by 2 to present two wave periods.

It is visible that the period optimum seems to shift slightly in these two minutes. This shift could

be caused by electronic drifts of the AOM driver. In an experimental setting, this would not cause that much of a problem, as the timescales which are interesting for the experiment are in the 100 ms regime.

3.6 Phase shift through EOM

In the last stage of characterizing the setup, an EOM was built into the experiment to imitate an atomic sample, in which the beam in one interferometer arm picks up a phase due to passing through an atomic cloud. Here, the phase shift is created by modulation in the EOM. The performance of detecting this phase shift is discussed in this section.

3.6.1 Probe signal

The EOM was operated with a 1 Hz, 250 V square signal. The evolution of the period over time is presented in figures 3.31 and 3.32. The histogram bin plots have been replaced by line plots of the histogram values. Figure 3.31 a one shows the accumulation of graphs at two phases, which are the phase without an EOM and the phase with a running EOM. The color ranging from blue to red indicates the folding at different times in the overall measurement sample from early to late. Figure 3.32 shows how the periodic signal behaves with the use of a heatmap, where the two different phases are visible through the stripe pattern. The setup is thereby capable of measuring a phase change applied to one of the interferometer arms.

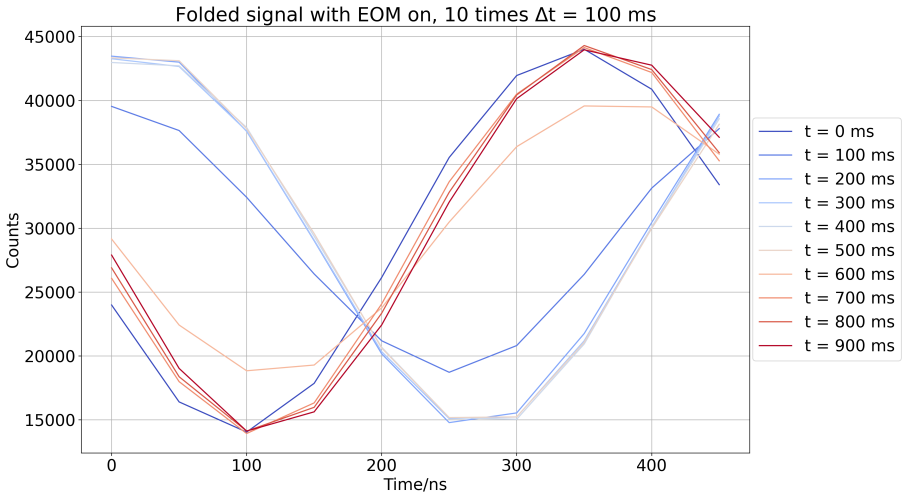

Figure 3.31: EOM applies a phase change to the probe arm light signal. Ten different time intervals of folded data with a length of 10 ms each are plotted. The color is ranging from red to blue and indicates the point in time in the measurement.

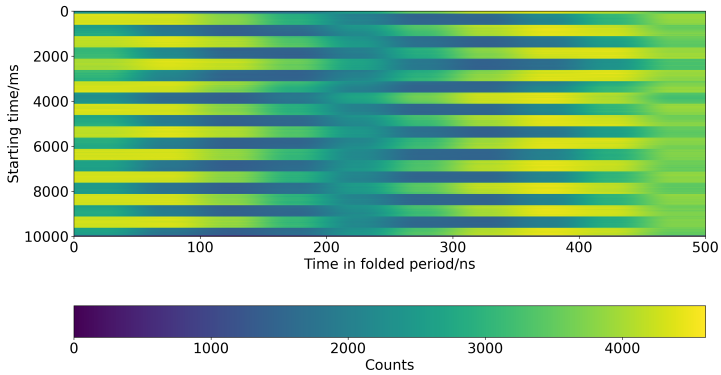

Figure 3.32: EOM applies a phase change to the probe arm light signal.

3.6.2 Relation between phase change and voltage control

How far the phase is shifted by the EOM can be controlled by the voltage applied. Because of the high voltage generator the voltage set in the function generator has to be multiplied by 50. To measure the relations, 6 different Voltages were set: 0 V, 1 V, 2 V, 3 V, 4 V, 5 V, which makes a range of 0-250 V applied. To extract the EOM-induced phase change a fit was made to the folded oscillating signals with the EOM off and with the EOM on. From these fits the phases were extracted and the difference was calculated. The result can be seen in figure 3.33.

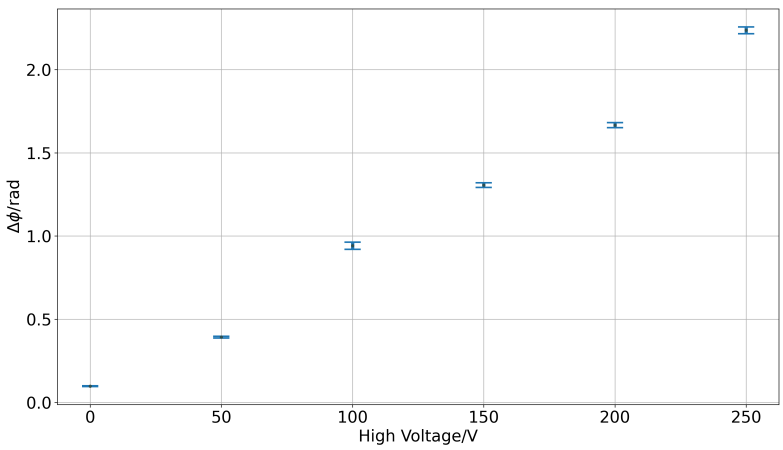

Figure 3.33: Phase change over the power of the EOM.

3.7 Noise

In section 2.2 it was discussed how the interferometer setup was enclosed in a box to minimize drifts due to the environment. To estimate the effect of this box, three measurements were taken. One was without any outer walls, the second was with the walls but missing the lid and the third was taken with the whole box in place. In figure 3.34 the results over different time lengths can be seen.

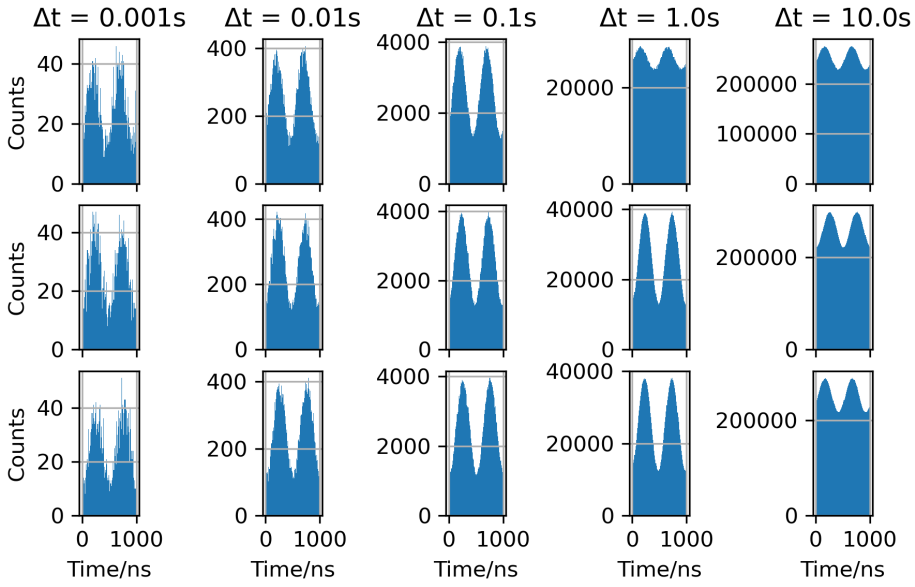

Figure 3.34: Different folding lengths for different box configurations per row. First row: without box, second row: without lid, third row: with whole box.

Without any outer walls, the signal washes out over longer timescales, but the two other measurements stayed stable up to 1 s. This showed that especially the side walls helped to reduce the outer influence primarily from airflow and make the setup more stable.

CHAPTER 4

Conclusion and outlook

In this thesis, an interferometer for measuring phase changes was built. The setup implemented a whole, functioning interferometer which produced a beat signal of around 2 MHz. This is created by the successful interference of two optical signals modulated with 80 MHz and 82 MHz respectively. The frequency modulations were produced with two acusto-optical modulator. The beat note was not only seen on a classical light level but also on a single photon level. The implementation of the single photon counting module and the Time Tagger showed the possibilities and current boundaries of the setup. The folding of the few appearing photons per period over longer time scales showed the appearance of a sinus wave with many iterations, for which a period was found. Testing this period on the supposed reference signal showed the unreliability of the relation between the electronic signal from two other outputs of the driver of the acusto-optical modulators compared to the modulation of the signal.

A period was also found for this signal, but it showed differences compared to the signal after the first decimal place. Additionally, this showed how severe the effects of a small change in the period number were on the folding at higher time scales. However, with a good fitting period the measurements showed a good stability even on timescales as large as 1 s. Here a periodic signal was visible and nearly as low as for 10 ms timescales. Over 10-100 s the contrast can wash out, depending highly on the chosen period. This period can change enough to make it less stable at a 1 s timescale.

To test the interferometer for its supposed use an electro-optical modulator was built in the setup to apply a phase change as an imitation of probing an atomic sample. Here a clear phase change was visible in the data, which showed that it works for this purpose. Moreover, the linear relation between the electro-optical modulator driving voltage and the applied phase shift was proven. Finally, the influence noise can have was made visible as the built box reduced the out washing effects at 1 s measurements. The box, especially the outer walls, makes the setup stable enough for 1 s phase measurements.

The biggest challenge during the experiment was the search for the period which is fundamental for the folding of the data. Here is room in the future for improvement as a phase change would always need a signal without the probe as a reference, where no other suitable option was found during the building process. With that in mind the interferometer is capable of measuring a phase shift.

For usage in a non-linear environment, there would be the need for a few adjustments of the setup. For instance, a splitter before the single photon counting module and a second detector detecting the other side are needed to condition the finding in one path to the measurement on the other. Additionally, there could be still made some improvements about finding a good period for the folding, as the measurements showed how crucial even small changes were for the measurement. Lastly, a suitable reference signal would need to be found. Here the optical reference beam could be tried out or some other way of getting a trigger signal, which would ease the problem with finding the exact, sensitive period since this would not be needed anymore.

Bibliography

[1] E. Hecht, *Optics*, eng, 4th ed, San Francisco: Addison-Wesley, 2002, ISBN: 978-0-321-18878-6 (cit. on pp. 1, 5).

[2] Daniel A. Steck, *Classical and Modern Optics*, 2003, URL: https://atomoptics.uoregon.edu/~dsteck/teaching/optics/optics-notes.pdf (cit. on p. 1).

[3] M. Fleischhauer, A. Imamoglu and J. P. Marangos, *Electromagnetically induced transparency: Optics in coherent media*, en, Reviews of Modern Physics **77** (2005) 633, ISSN: 0034-6861, 1539-0756, URL: https://link.aps.org/doi/10.1103/RevModPhys.77.633 (visited on 15/02/2023) (cit. on p. 1).

[4] T. Peyronel et al., *Quantum nonlinear optics with single photons enabled by strongly interacting atoms*, en, Nature **488** (2012) 57, ISSN: 0028-0836, 1476-4687, URL: http://www.nature.com/articles/nature11361 (visited on 15/02/2023) (cit. on p. 1).

[5] O. Firstenberg, C. S. Adams and S. Hofferberth, *Nonlinear quantum optics mediated by Rydberg interactions*, Journal of Physics B: Atomic, Molecular and Optical Physics **49** (2016) 152003, arXiv:1602.06117 [quant-ph], ISSN: 0953-4075, 1361-6455, URL: http://arxiv.org/abs/1602.06117 (visited on 14/02/2023) (cit. on p. 1).

[6] D. Tiarks, S. Schmidt, G. Rempe and S. Dürr, *Optical phase shift created with a single-photon pulse*, en, Science Advances **2** (2016) e1600036, ISSN: 2375-2548, URL: https://www.science.org/doi/10.1126/sciadv.1600036 (visited on 15/02/2023) (cit. on p. 1).

[7] M. D. Lukin et al., *Dipole Blockade and Quantum Information Processing in Mesoscopic Atomic Ensembles*, en, Physical Review Letters **87** (2001) 037901, ISSN: 0031-9007, 1079-7114, URL: https://link.aps.org/doi/10.1103/PhysRevLett.87.037901 (visited on 15/02/2023) (cit. on p. 1).

[8] E. Brion, K. Mølmer and M. Saffman,
Quantum Computing with Collective Ensembles of Multilevel Systems, en,
Physical Review Letters **99** (2007) 260501, ISSN: 0031-9007, 1079-7114,
URL: https://link.aps.org/doi/10.1103/PhysRevLett.99.260501 (visited on
15/02/2023) (cit. on p. 1).

[9] Q. A. Turchette, C. J. Hood, W. Lange, H. Mabuchi and H. J. Kimble,
Measurement of conditional phase shifts for quantum logic,
(1995), Publisher: arXiv Version Number: 1,
URL: https://arxiv.org/abs/quant-ph/9511008 (visited on 15/02/2023) (cit. on p. 1).

[10] O. Firstenberg et al., *Attractive photons in a quantum nonlinear medium*, en,
Nature **502** (2013) 71, ISSN: 0028-0836, 1476-4687,
URL: http://www.nature.com/articles/nature12512 (visited on 15/02/2023)
(cit. on p. 1).

[11] Marian Rockenhäuser, *A Setup for Heterodyne Single-Photon Phase Shift Detection*,
Bachelorthesis: University of Stuttgart, 2016, URL: https://www.nqo.uni-
bonn.de/publications/2016-marian-rockenhauser-bachelor.pdf (cit. on p. 1).

[12] Mikkel Gaard Hansen, *Precision Measurements in a Rydberg Quantum Optics Experiment*,
MA thesis: University of Southern Denmark, 2021, URL: https://www.nqo.uni-
bonn.de/publications/2021-mikkel-gaard-hansen-master-thesis.pdf
(cit. on pp. 1, 11).

[13] Tomer Zohar, *Attractive photon interactions and bound states mediated by an ensemble of cold Rydberg atoms*, MA thesis: Weizmann Institute of Science, 2021 (cit. on pp. 1, 3).

[14] L. Drori et al., *Quantum vortices of strongly interacting photons*, tech. rep. arXiv:2302.05967,
arXiv:2302.05967 [physics, physics:quant-ph] type: article: arXiv, 2023,
URL: http://arxiv.org/abs/2302.05967 (visited on 16/02/2023) (cit. on p. 1).

[15] M. Fox, *Quantum optics: an introduction*, Oxford master series in physics 15,
Oxford ; New York: Oxford University Press, 2006,
ISBN: 978-0-19-856672-4 978-0-19-856673-1 (cit. on pp. 4, 24).

[16] D. Meschede, *Optics, Light and Lasers: The Practical Approach to Modern Aspects of Photonics and Laser Physics*, en, 1st ed., Wiley, 2006,
ISBN: 978-3-527-40628-9 978-3-527-61887-3,
URL: https://onlinelibrary.wiley.com/doi/book/10.1002/9783527618873
(visited on 15/02/2023) (cit. on pp. 6, 9).

[17] Swabian Instruments, *Time Tagger User Manual*, tech. rep., 2022, URL: https://www.
swabianinstruments.com/static/downloads/TimeTagger_User_Manual.pdf
(cit. on p. 9).

[18] Swabian Instruments, *Streaming time-to-digital converter*, 2023, URL: https:
//www.swabianinstruments.com/static/downloads/TimeTaggerSeries.pdf
(cit. on p. 9).